Numerical Modelling of Porous Radiant Burners Using Full and Reduced Kinetics Mechanisms

Khosravy El-Hossaini, Mostafa; Maerefat, Mehdi*+; Mazaheri, Kiumars
Department of Mechanical Engineering, Faculty of Engineering, Tarbiat Modares University, P.O. Box 14115-111 Tehran, I.R. IRAN

ABSTRACT: *The present paper compares full kinetics mechanisms in numerical modelling of porous radiant burners (PRB), with their reduced forms. The two most frequently used mechanisms of methane combustion (GRI3.0 and Miller) were selected and their effects were examined on temperature, species concentration, burning speed, and pollutant emission. While the findings of numerical simulation of PRB show fine concurrence between each full mechanism and its related reduced mechanism, no significant temperature differences are observed in the results of full mechanisms. However, CO concentration along burner axis shows a small difference between two full mechanisms, which is related to HCO and HO_2 concentrations. The inconsistency is more pronounced for NO concentration along porous axis, which is due to prompt NO evaluation. The present research finds deviation also between burning speeds, calculated by numerical simulation and experimental results. This difference is much more significant in rich mixtures. GRI3.0 mechanism estimated the burning velocities as closer to the experimental values than those predicted using Miller mechanism.*

KEY WORDS: *Full kinetics mechanism, Reduced mechanism, Porous radiant burner, Numerical simulation.*

INTRODUCTION

Since the last decade, there has been significant increase in the combustion of hydrocarbon fuels, especially methane, within porous inert medium. Most of the previous studies had used single step global chemistry as an engineering approach. Also, during the last decades, there prevailed multi-step kinetics to predict temperature distribution, burning speed and pollutant emissions; of course, each of them has its own limitations on parameters like temperature and pressure range and therefore, special care is needed when such models are applied to the process. Because of energy exchange from gas to solid phases, porous inert burners have specific temperature distribution, which is one of the main reasons of difference between them and ordinary burners. As such, there needs a special care to select a combustion mechanism for porous radiant burners modelling.

Heat transfer is enhanced by absorbent matrix in porous burners, consequently leading to increase its power density. In the combustion process, fuel releases heat in a small region and then it is transferred to other

* *To whom correspondence should be addressed.*
+ *E-mail: Maerefat@modares.ac.ir*
1021-9986/08/1/53 11/$/3.10

zones by conduction and radiation. The heated porous matrix preheats inlet mixture of fuel/air by convection. Depending on the amount of heat re-circulation, the burner may extend the flammability limits of lower heating value fuels and leaner mixtures, which might facilitate high rate of reaction leading to augment laminar flame speeds of mixture entering the burner. At the same time, heat could be efficiently transported out of the combustion chamber by the good thermal properties of porous matrix. This makes possible to control the combustion process in temperature and adjust it to minimize emission of pollutants like CO and NOx.

Due to the specific characteristics of combustion and heat transfer inside porous media, it is worthy to examine the validity of combustion mechanisms, which are proposed for free flames. The use of multi-step kinetics, according to *Hsu* and *Matthews*, is crucial to predict the temperature distribution, species profiles and other parameters of PRB [1].

In another research, *Zhou* and *Pereira* compared the accuracy of four combustion mechanisms: *Miller* full mechanism, Skeletal and 4-step reduced mechanisms (which are based on *Miller* mechanism), and 1-step global mechanism [2] and con-cluded that the 4- step reduced mechanism satisfactorily agrees with the full mechanism in combustion simulation in porous media. On the basis of GRI 2.1 and its 10-step reduced mechanisms, *Diamantis et al.* developed a numerical model for planar premixed flame of methane in ceramic porous media [3]. Other researchers used either of the two full mechanisms i.e. GRI or *Miller*, for combustion simulation in porous media. Comprehensive reviews of the earlier studies on PRBs are given by *Howell* [4] and *Viskanta* [5].

Since, GRI and *Miller* mechanisms have been used as common combustion mechanisms in PRBs modelling, therefore, the present work intends to compare these two mechanisms for modelling the combustion in porous ceramics. Also, it tries to validate the corresponding reduced mechanisms for the numerical simulation of PRBs. Further, due to the involvement of complex calculation and enormous computation cost for full chemical kinetics mechanisms, it has always been very attractive to use simple kinetics mechanisms or the so-called reduced mechanisms. These comparisons are made on the basis of the findings of operational characteristic like temperature, species profiles and flame speed.

Governing Equations

During the course of this study, we assumed a one-dimensional geometry, inert homogeneous porous material, constant properties and constant pressure. Since, the current paper aims to concentrate on the chemical kinetics mechanisms; side heat transfer is neglected. To predict the superficial characteristics along porous medium, the volume averaging method is used. Thus the volume averaged governing equations are:

Mass conservation

$$\frac{\partial(\rho_g \phi)}{\partial t} + \frac{\partial(\rho_g U \phi)}{\partial x} = 0 \qquad (1)$$

Species conservation

$$\rho_g \phi \frac{\partial Y_k}{\partial t} + \rho_g U \phi \frac{\partial Y_k}{\partial x} + \frac{\partial}{\partial x}\left(\rho_g \phi Y_k V_k\right) - \phi \dot{\omega}_k W_k = 0 \qquad (2)$$

Gas phase energy conservation

$$\rho_g C_{p,g} \phi \frac{\partial T_g}{\partial t} + \rho_g U C_{p,g} \phi \frac{\partial T_g}{\partial x} - \frac{\partial}{\partial x}\left(\phi k_g \frac{\partial T_g}{\partial x}\right) + \qquad (3)$$

$$\phi \sum_{k=1}^{N} \rho Y_k V_k C_{p,k} \frac{\partial T_g}{\partial x} + \phi \sum_{k=1}^{N} h_x \dot{\omega}_k + H_v\left(T_g - T_s\right) = 0$$

Solid phase energy conservation

$$\rho_s C_{p,s}(1-\phi)\frac{\partial T_s}{\partial t} + \frac{\partial}{\partial x}\left((1-\phi) k_s \frac{\partial T_s}{\partial x}\right) + \qquad (4)$$

$$H_v\left(T_g - T_s\right) - \frac{dq_r}{dx} = 0$$

In these equations, ϕ is porosity, U is flow velocity, H_v is volumetric heat transfer coefficient and k_s is conduction heat transfer coefficient. Also Y_k, V_k, $\dot{\omega}_k$, W_k and h_k are mass fraction, diffusion velocity, mole generation rate, molar weight and absolute enthalpy of species k, respectively. Further, subscripts *g* and *s* denote gas and solid phases, respectively.

A single layer porous burner is selected for the study (Fig. 1), which is made of 10.16 cm thick reticulated zirconia. The thermo-physical properties of porous matrix is shown in table 1. The volumetric heat transfer coefficient is assumed to be constant [1,2].

There are two approaches to premix flame simulation: burner stabilized flame and free propagating flame. The first is often used to analyze species profiles in flame

Table 1: Thermo-physical properties of porous matrix model [6].

$\beta = 270\ m^{-1}$	$\sigma_S = 216\ m^{-1}$
$H_v = 10^7\ W / m^3\text{-}K$	$k_S = 1.2\ W / m\text{-}K$
$\rho_S = 5.56 \times 10^3\ kg / m^3$	$\phi = 0.87$ for 3.9 PPC PSZ
$c_{p,s} = 824\ J / kg\text{-}K$	

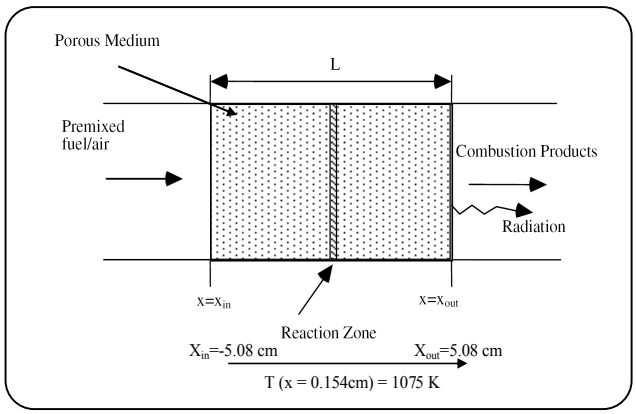

Fig. 1: Schematic of porous radiant burner.

experiments with already identified rate of mass flow, whereas, the latter is used to predict flame speed along burner axis with identified temperature of one point. The second approach is followed in the present study, with fixing temperature of one point in preheating zone.

Boundary Conditions

The species mass fractions are usually known at the inlet of the domain (x = xin), where the gas temperature enforces all heat conducted upstream to advert back into the left of computational domain (Eq. (5)).

$$\dot{m}c_{p,g}\left(T_{g,i} - T_g\right) = -k_g \frac{\partial T_g}{\partial x} \quad \text{at} \quad x = 0 \tag{5}$$

The temperature gradient is put to zero at the outlet (Eq. (6)) [7].

$$\frac{\partial T_g}{\partial x} = 0 \quad \text{at} \quad x = L \tag{6}$$

The solid phases (both inlet and outlet) are subjected to transfer convective heat to gas and exchange radiation with the surrounding. It is assumed that surround temperatures are same as gas temperature at burner sides. So the energy equation of solid at foam surface reduces to:

$$\left[h_i\left(T_{g,i} - T_s\right) + \sigma\varepsilon_i\left(T_{i,surround}^4 - T_s^4\right)\right](1-\phi) = -k_{eff,s}\frac{\partial T_s}{\partial x} \quad \text{at} \quad x = 0 \tag{7}$$

$$\left[h_o\left(T_{g,o} - T_s\right) + \sigma\varepsilon_o\left(T_{o,surround}^4 - T_s^4\right)\right](1-\phi) = -k_{eff,s}\frac{\partial T_s}{\partial x} \quad \text{at} \quad x = L \tag{8}$$

Where, h_i and h_o are convective heat transfer coefficients at inlet and outlet, respectively and equal to 500 W/m^2s and as such $k_{eff,s} = (1-\phi)k_s$ is effective thermal conductivity of solid.

To close the problem, it needs radiative transfer equation that allows calculating radiation intensity, which has been shownd in Eq. (4). The radiant flux is solved using the discrete ordinates method [8].

The Solution Method

To solve the above-mentioned partial differential equation subjected to the specified boundary condition, the PREMIX code of the CHEMKIN package [9] is applied with some modifications. Firstly, we calculated species profiles using a pre-defined temperature distribution. In this step, temperatures of solid and gas are in thermal equilibrium. Secondly, we implicitly solved species conservation, solid and gas energy equations. Lastly, a calculation was made on radiation source term of solid energy equation and temperature profile was modified. The second step is re-iterated until the desired convergence is obtained.

CHEMICAL KINETICS MECHANISMS

Miller Mechanism

Miller et al. proposed this mechanism for methane combustion in 1989. The full reaction scheme comprises 49 species and 227 elementary reactions. Due to the limitation of space, it is impossible to list complete reaction mechanism that consists of oxidation mechanism for C1 and C2-hydrocarbons, HCN and NH_3, along with a subset describing the interaction between hydrocarbon species and the nitrogen chemistry [10].

GRI-Mech 3.0

It is an optimized detailed chemical reaction mechanism that represents current best underestanding of natural gas combustion including NOx formation and

re-burn chemistry. It consists of 325 elementary reactions and associated rate coefficients as well as thermo-chemical parameters for 53 chemical species. Apart from propane and C2 oxidation species, it has included new formaldehyde (CH_2O), NO formation and re-burn chemistry, as well [11].

Reduced Mechanism Based on Full Miller Mechanism

Homma and *Chen* have applied the quasi steady state (QSSA) on 28 species(C, C_2H, CH, CH_2(s), NNH, CN, N, H_2CN, HCCO, NH, CH_2, NH_2, HCO, NCO, C_2H_3, CH_2OH, NH_3, CH_3O, C_2H_5, HOCN, CH_2CO, HNO, HCCOH, HNCO, HCNO, N_2O, H_2O_2 and HCN). Further, they have also developed a 16-step reduced mechanism, in order to assess the validity of QSSA on H_2O_2 and HCN. Consequently, it was found that reduced mechanism contains 16 reactions in 20 species, which are follows [12].

$CH_4 + H = CH_3 + H_2$ (M1)

$CH_4 + OH = CH_3 + H_2O$ (M2)

$CH_4 + O_2 = CH_3 + HO_2$ (M3)

$2CH_4 + C_2H_2 = 2C_2H_4 + H_2$ (M4)

$CH_3 + H = CH_4$ (M5)

$2CH_3 = C_2H_6$ (M6)

$CH_3 + O = CH_2O + H$ (M7)

$CH_3 + O_2 = CH_2O + OH$ (M8)

$CH_3 + O + HO_2 = CH_2O + 2OH$ (M9)

$2CH_3 + 2OH = H_2 + 2H_2O + C_2H_2$ (M10)

$2O + C_2H_2 = 2CO + H_2$ (M11)

$2CO + 2H_2 + 2O + 2OH + N_2 = 4H + 2O_2 + C_2H_2 + 2NO$ (M12)

$4CO + 2H_2 + 2OH + N_2 = 2CO_2 + 4H + C_2H_2 + 2NO$ (M13)

$2CO + 3H_2 + 2NO = 4H + C_2H_2 + 2NO_2$ (M14)

$CH_4 + HO_2 = CH_3 + H_2O_2$ (M15)

$C_2H_2 + N_2 = 2HCN$ (M16)

Reduced Mechanism Based on GRI3.0

An augmented reduced mechanism (ARM) for 15-steps and 19-species, based on GRI-Mech 3.0, was shown to be adequate for methane oxidation at global level as well as detailed flame structure [13]:

$CH_4 + H = CH_3 + H_2$ (G1)

$CH_3 + OH = CH_2O + H_2$ (G2)

$CH_2O = CO + H_2$ (G3)

$C_2H_6 = C_2H_4 + H_2$ (G4)

$C_2H_4 + OH = CH_3 + CO + H_2$ (G5)

$C_2H_2 + O_2 = 2CO + H_2$ (G6)

$CO + OH + H = CO_2 + H_2$ (G7)

$H + OH = H_2O$ (G8)

$2H_2 + O_2 = 2H + 2OH$ (G9)

$2H = H_2$ (G10)

$HO_2 + H = H_2 + O_2$ (G11)

$H_2O_2 + H = H_2 + HO_2$ (G12)

$N_2 + O_2 = 2NO$ (G13)

$HCN + H + O_2 = H_2 + CO + NO$ (G14)

$NH_3 + 3H + H_2O = 4H_2 + NO$ (G15)

In this mechanism, (G1) to (G3) represent the conversion of $CH_4 \rightarrow CH_3 \rightarrow CH_2O \rightarrow H_2$ & CO, (G4) to (G6) account to form C_2 species such as, C_2H_6, C_2H_4, and C_2H_2, and their subsequent oxidation. (G7) and (G8), respectively correspond to CO_2 and H_2O formations as well as (G9) - (G12) relate to the sub-mechanism of H_2 oxidation including the chemistry of HO_2 and H_2O_2. (G13) includes NO formation reaction corresponding to thermal NO, prompt NO, and the N_2O-intermediate. In addition, reactions between nitrogen-related radicals and N/NO, converting N and NO back to N_2, are also accounted for. Moreover, (G14) involves the prompt and re-burning reactions whereas (G15) shows NH_3 reaction.

RESULTS AND DISCUSSION

Temperature Profiles

Fig. 2 shows the temperature distribution along the burner axis (central area), comparing the results of four combustion mechanisms in porous media. Since volumetric heat transfer coefficient is large, the temperature of

solid and gas phases overlap each other except on a small area in preheat zone.

There are very good agreements between reduced mechanisms with their corresponding full mechanisms. However, a small disparity is observed between two full mechanisms. The difference is about 20 Kelvin in outlet boundary, while the peak difference, about 125 degree Kelvin, appears just after combustion zone.

The temperature profile of lean combustion (λ=0.6) has been shown is Fig. 3. The temperature distributions along porous axis of four combustion mechanisms show approximately similar behavior with a maximum gap of 30 Kelvin between GRI3.0 and Miller. Very similar behavior of temperature profiles is observed for rich mixtures, as well.

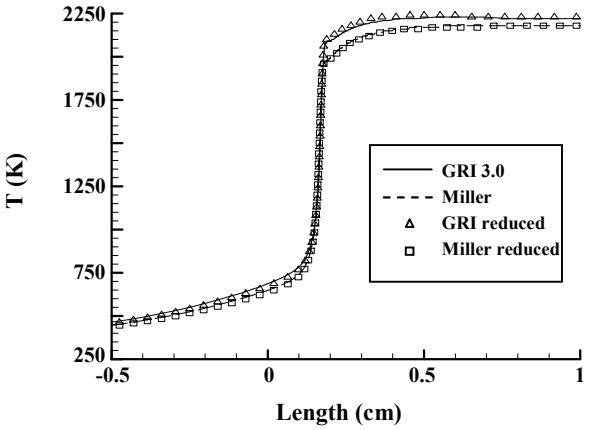

Fig. 2: Temperature profile of porous radiant burner for stoichiometric methane-air mixture (λ=1) and prescribed temperature T(0.157 cm) = 1075 K.

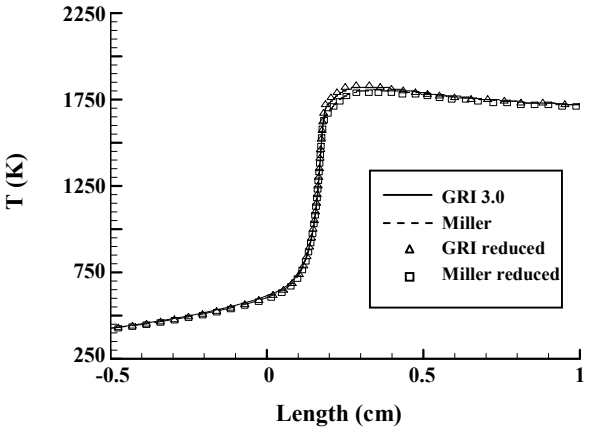

Fig. 3: Temperature profile of porous radiant burnerat lean mixture (λ=0.6) and prescribed temperature T(0.157 cm) = 1075 K.

CO Emission

The CO formation occurs during the rapid fuel consuming reactions in the primary reaction zone of hydrocarbon flames [14]. In primary flame zone, CH_x species react much faster than CO with oxidizing radicals. It means, CO cannot be oxidized until the gas exits from this primary zone as well as CH_x level drops significantly. Consequently, the slow oxidation process of CO at the secondary zone kinetically, is a limited process of interest in lean premixed combustion. Several elementary reaction steps have been taken out from Miller and GRI mechanisms, responsible to predict CO emissions in lean premixed combustion:

$$HCO + M = H + CO + M \quad (R1)$$

$$HCO + O_2 = HO_2 + CO \quad (R2)$$

$$CO + OH = CO_2 + H \quad (R3)$$

$$HCO + OH = H_2O + CO \quad (R4)$$

Although, these reactions are common in both full mechanisms, however, there appear only differences in rate constants. The hydrogen-contained species in these elementary reactions strongly influence the burnout characteristics of CO [14].

Fig. 4 shows CO mole fraction profile along the axis of the burner. There appears little difference between the results of two mechanisms. Fig. 3 shows two sets of curves for two different equivalent ratios. The general trend is almost the same. For equivalent ratio 0.6, two mechanisms predict the climax of CO concentration at

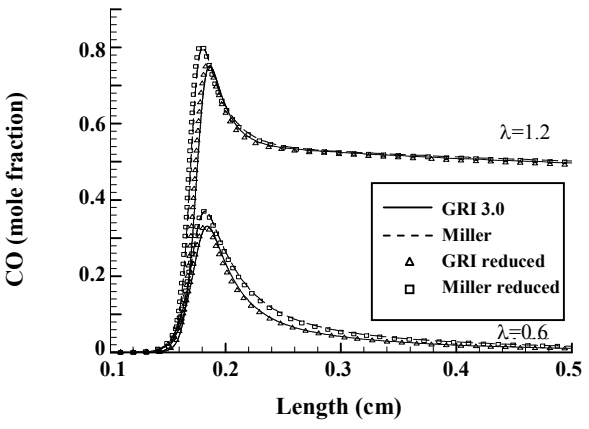

Fig. 4: CO mole fraction profile for equivalence ratio 0.6 and 1.2.

almost similar position. GRI3.0 predicts a peak value of about 0.0329 at x=0.1842 cm whereas, the corresponding value for modelling with *Miller* mechanism is 0.0376 at x=0.1833 cm. For rich mixtures, almost same behavior is observed in CO concentration profiles. Results indicate that both reduced mechanisms closely follow their corresponding full mechanisms.

Figs. 5 through 7 compare the mole fraction profiles of species, taking part in reactions (R1) - (R4) for two full mechanisms. As shown, there is no significant difference between H, OH and CH_3 species profiles at $\lambda = 0.6$. However, Figs. 8 and 9 show some of the differences of HCO and HO_2 mole fraction profiles along burner axis for this mixture. With reference to rich combustion, CH_3 and H as well as HCO and HO_2 affect CO prediction in both full mechanisms.

NO Emission

Another important phenomenon of practical interest in lean premixed flame is the formation of NO_x, a reaction occurring at much slower rates than the main heat release reactions. NO in methane flames is formed by three mechanisms i.e. thermal, N_2O intermediate and prompt mechanisms. Sensitive to temperature fluctuations and significant only at high temperatures, the thermal NO, principally, is formed from the reactions involving N and O atoms:

$$O + N_2 = NO + N \quad (R5)$$

$$N + O_2 = NO + O \quad (R6)$$

$$N + OH = NO + H \quad (R7)$$

The N_2O-intermedate mechanism has been considered a significant contributor to NO in lean premixed systems and can be described by following elementary reactions [14]:

$$N_2 + O + M = N_2O + M \quad (R8)$$

$$N_2O + H = N_2 + OH \quad (R9)$$

$$N_2O + O = N_2 + O_2 \quad (R10)$$

$$N_2O + O = NO + NO \quad (R11)$$

Forming as an intermediate (R8), N_2O is then converted to NO (R11) and leads to N_2 once attacked by H and O atoms (R9 and R10). The N_2O mechanism is more important than thermal NOx at low temperatures.

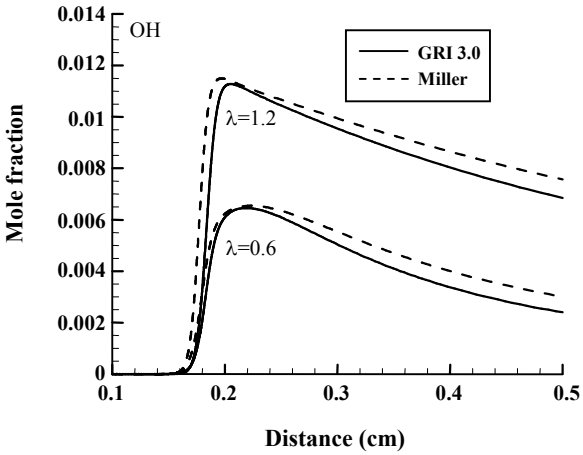

Fig. 5: OH mole fraction along burner axis.

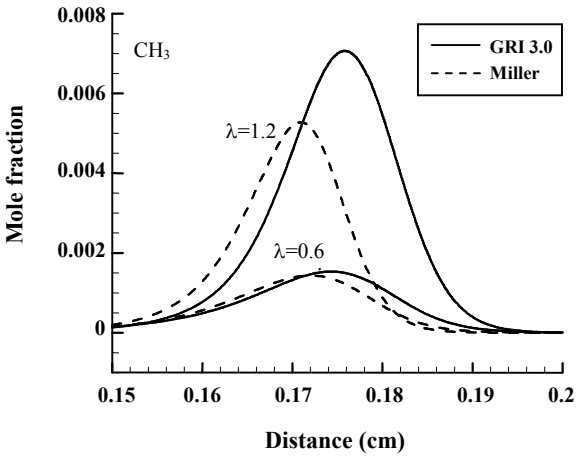

Fig. 6: CH3 mole fraction along burner axis.

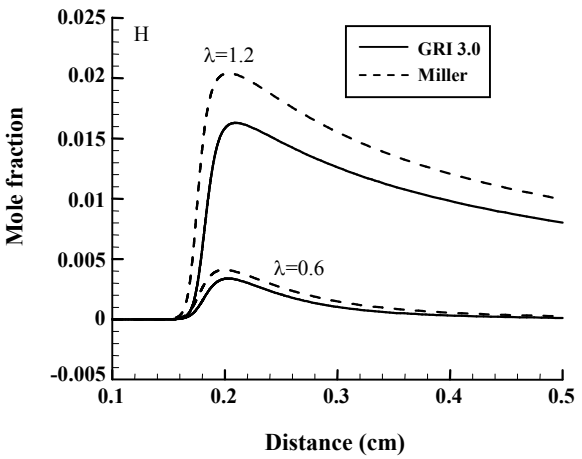

Fig. 7: H mole fraction along burner axis.

Prompt NOx is formed from cyano species and N atoms oxidation, which are further formed from hydro-carbon radicals in the flame zone:

$$CH + N_2 = HCN + N \quad (R12)$$

The oxidation of the HCN molecules to NO follows the reactions sequence of HCN→CN→NCO→NO and the oxidation of N and NO is mainly governed by reaction (R6). *Glarborg* has showed OH concentration effect in NO production [15].

$$CO + OH = CO_2 + H \quad (R13)$$

$$H + O_2 = OH + O \quad (R14)$$

$$H + O_2 + M = HO_2 + M \quad (R15)$$

Reactions (R5) to (R15) are repeated in both full mechanisms. The only differences appear in the rate constants. Figs. 10-12 show NO profiles for three mixtures i.e. lean, stoichiometric and rich mixtures. With respect to CO predictions, the differences between two mechanisms are much more pronounced here. The agreement between full and their corresponding reduced mechanisms is not as satisfactory as CO and temperature predictions. Particularly, this difference is noticeable for GRI3.0 mechanism, due to grid points of two types of mechanisms, which have already been discussed in section (4-4). Hence, GRI3.0 predicts higher value of NO than those of *Miller* mechanism.

The gap between the results of GRI3.0 and *Miller* mechanisms might attribute to three types of NO formations. Fig. 12 shows mixture fraction profiles of O, H, OH, N_2O species, which play critical role in thermal NO and N_2O-intermediate reactions. The path of prompt NO formation may be found with HCN and N mole fraction variation in two mechanisms, shown in Figs. 14-19.

Figs. 14 to 19 indicate that the predicted N and HCN from GRI3.0 differ from those obtained applying Miller mechanism, and thus highlight the difference in NO predictions for two mechanism roots on prompt NO reactions.

Comparison with Experimental Data

Fig. 20 shows CO mole fractions at burner outlet for different equivalent ratios. The computed value is compared with the experimental data taken from

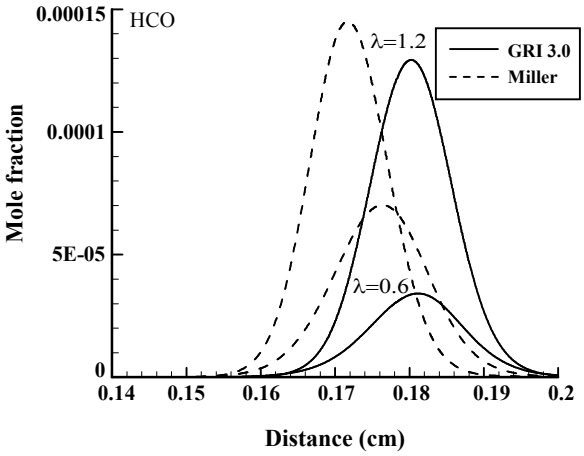

Fig. 8: HCO mole fraction along burner axis.

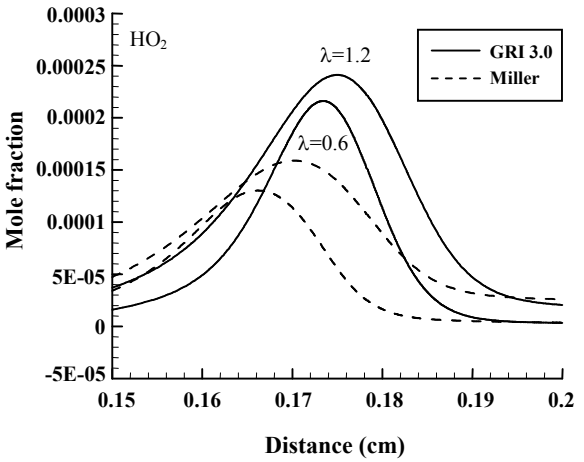

Fig. 9: HCO mole fraction along burner axis.

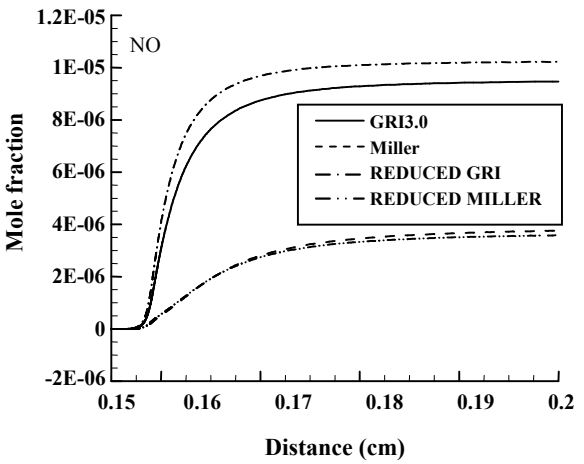

Fig. 10: NO mole fraction along burner axis at λ=0.6.

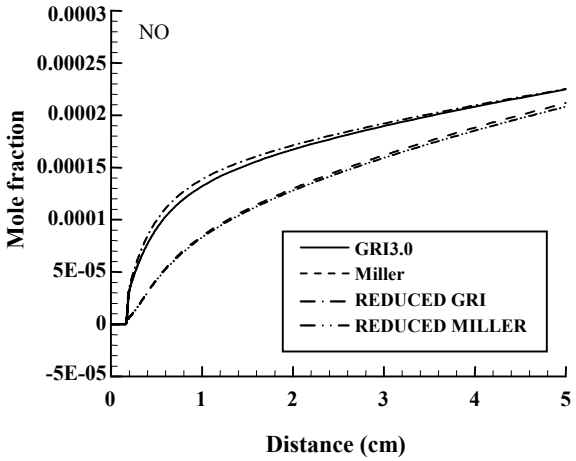

Fig. 11: NO mole fraction along burner axis at λ = 1.0.

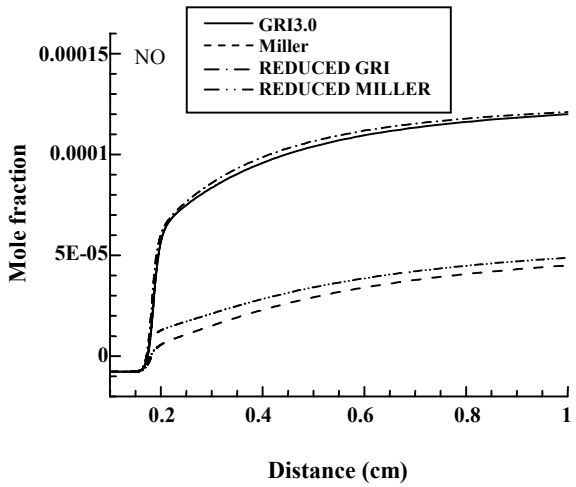

Fig. 12: NO mole fraction along burner axis at λ = 1.2.

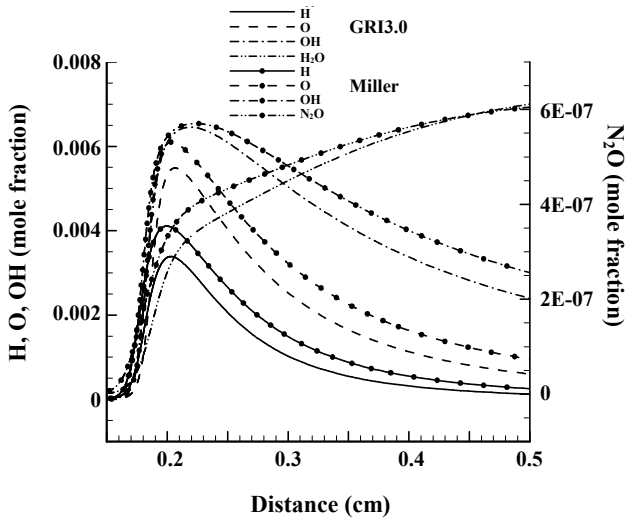

Fig. 13: O, H, OH, N_2O mole fractions along burner axis at λ = 0.6.

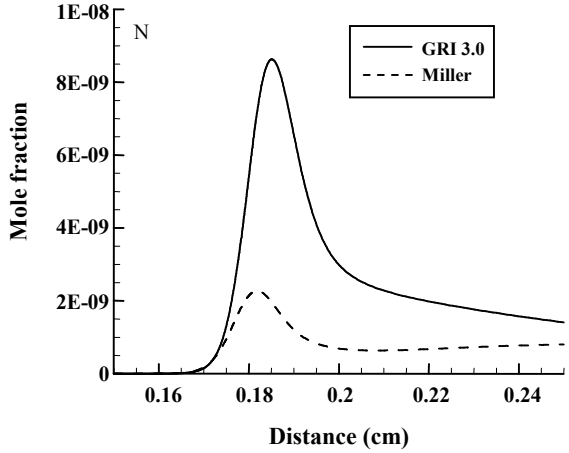

Fig. 14: N mole fractions along burner axis at λ = 0.6.

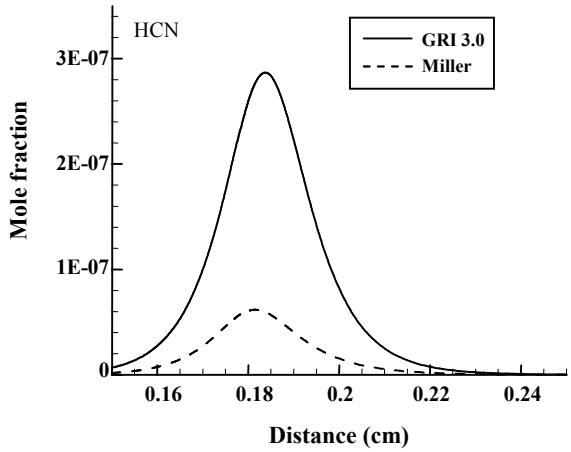

Fig. 15: HCN mole fractions along burner axis at λ = 0.6.

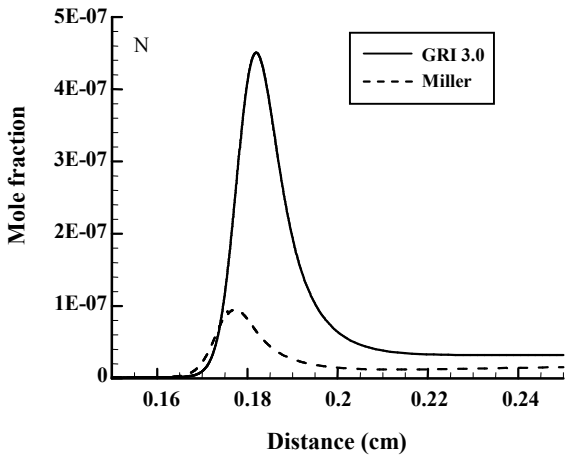

Fig. 16: N mole fractions along burner axis at λ = 1.0.

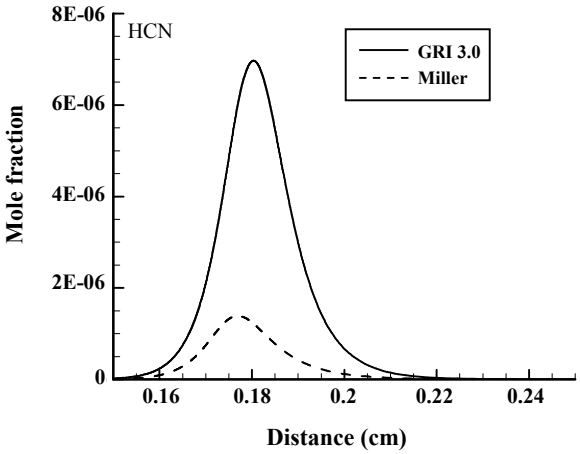

Fig. 17: HCN mole fractions along burner axis at λ = 1.0.

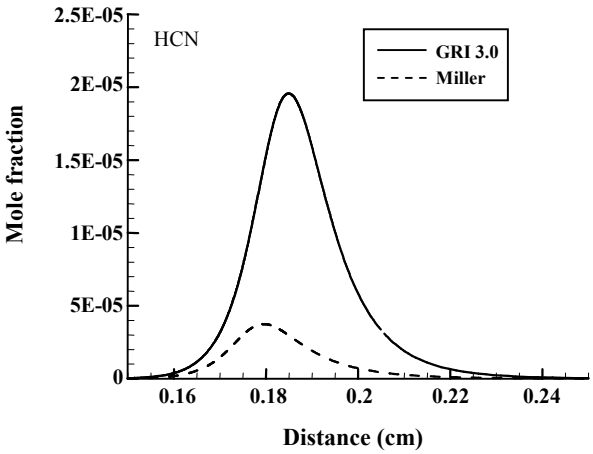

Fig. 19: HCN mole fractions along burner axis at λ = 1.2.

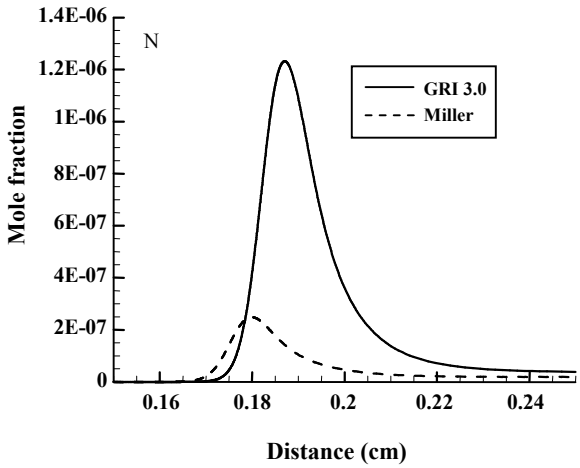

Fig. 18: N mole fractions along burner axis at λ = 1.2.

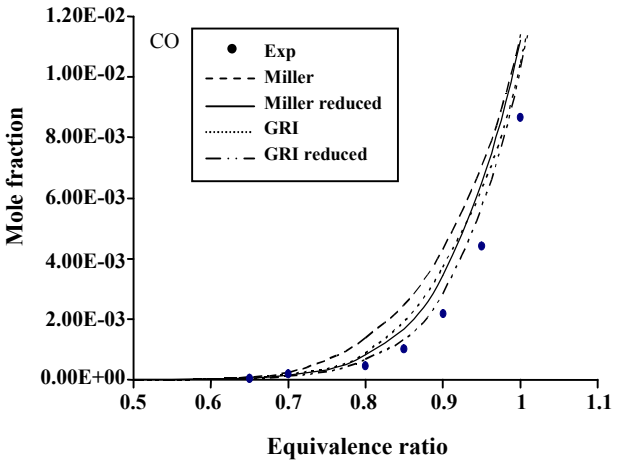

Fig. 20: Comparison of the results of numerical simulation with experimental data for CO.

reference [6]. Generally there exists agreement but GRI3.0 mechanism shows better estimate than *Miller* mechanism. The deviations of reduced mechanisms to that of full mechanisms are due to grid point finesse where the points used for detailed and reduce mechanisms are 350 and 1000, respectively. In the case of detailed mechanism, the calculation with more grid points is computationally prohibitive.

Unlike porous combustion, the simulation of a free flame does not need too much grid points. It needs about 100 computational points, however, porous medium combustion needs up to 1000 node to obtain a grid independent solution for full GRI3.0.

Fig. 21 shows NO mole fractions as a function of equivalent ratio at the burner outlet. The numerical findings of *Hsu* and *Matthews* are also shown in this figure. It is observed that numerical simulations predict value that is much higher than the experimental reference [6] data. Since, *Hsu et al.* considered only thermal NO, their calculated NO mole fractions are smaller than our findings. The small differences between full and reduced mechanisms are due to the different number of grid points, used in different cases. To examine this reason, the calculation is repeated up to 880 grid points at stoichiometric mixture for full mechanisms. Figs. 20 and 21 indicate that with increasing grid points in reduced mechanisms, results become closer to experimental data than those of full mechanisms.

A part of the discrepancy between our predictions and the experimental data might lead to more fundamental problems with the models, employed in present study. For instance, our understanding about thermal radiation and fluid mechanical processes within porous media is far from being complete. On the other hand, there are some important uncertainties with regard to solid properties, used in our calculations [4]. The NO formation is closely connected with temperature profile, and temperature profile is strongly influenced by conductive, radiative, and convective heat transfer in porous media [2]. In more compicated two dimensional modeling, it is shown that heat loss from circumferential wall can reduce flame peak temperature and also reduce NO production [16].

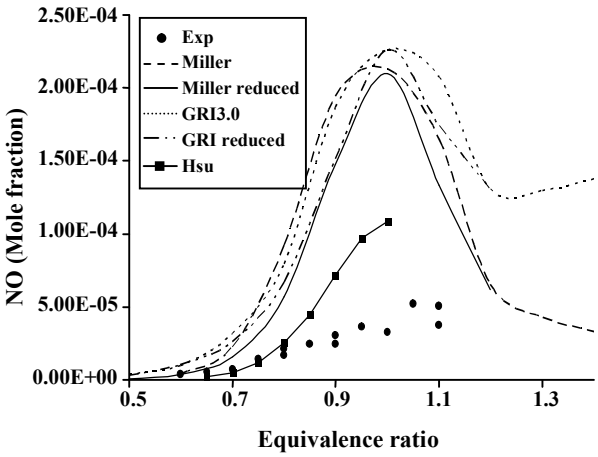

Fig. 21: Comparison of the results of numerical simulation with experimental data for NO.

Burning Speed

Burning speed or firing rate is one of the most important parameters of burners. The burning speed is defined as the average velocity of the cold unburned gases, just ahead of the burner inlet. Fig. 22 shows almost the same predicted burning speeds obtained with the two full mechanisms as a function of equivalent ratio and generally the trends have found the same for both full mechanisms. However, the *Miller* mechanism predicts slightly higher values for rich mixtures, which is due to the higher temperature predictions. Fig. 22 also indicates the results of *Hsu, et al.* calculations as well as the experimental data of reference [6]. Obviously, none of these simulations can predict a satisfactory value for the burning speed. This discrepancy may be due to the limited knowledge of the fundamentals of thermal, radiative, and fluid mechanical processes within porous media.

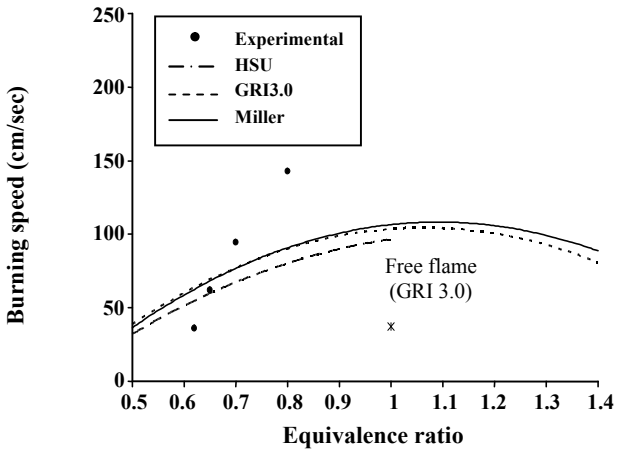

Fig. 22: Comparison of burning speed.

Computational Cost

The computaion time (CPU time) is one of the most important parameters in a numerical simulation. In combustion simulation, the main reason of using a reduced mechanism is the CPU time saving. Fig. 23 shows convergence time for GRI3.0 full mechanism and its corresponding reduced mechanism. It is observed that the computational cost is much higher for the full mechanism. In both cases, time is increased almost linearly with increasing the number of grid points. The variation slope is much higher for full mechanism.

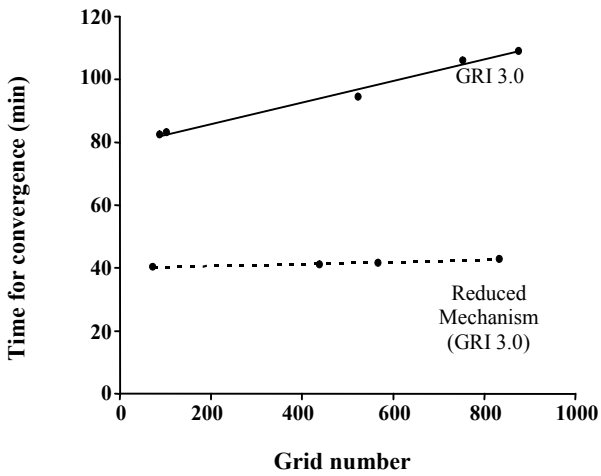

Fig. 23: Comparison of the convergence times of the porous burner simulation using GRI3.0 and its corresponding 15-step reduced mechanism (stoichiometric mixture).

However, reduced mechanism improves the computational expense for a grid free solution.

CONCLUSIONS

Numerical simulation results of porous media combustion show full agreement between detailed mechanisms and their corresponding reduced mechanisms. However, a considerable computational time saving was observed for reduced mechanisms. With regard to temperature distribution, all mechanisms predict almost the same profile. The CO mole fraction profiles of full mechanisms show a little variation due to difference in kinetic rate constants, resulting different HCO and HO_2 mole fractions. In rich mixtures, species that affect CO formation are: HCO, HO_2, H, and CH_3. The CO concentration obtained by numerical simulation is in agreement with experimental data. While comparing with experimental data, the NO concentration is over-predicted. There are two intrinsic sources for this difference, i.e. uncertainties on heat transfer coefficients and heat losses from wall side. In addition, there has also observed considerable difference between two full mechanisms so far as NO mole fraction is concerned. It is argued that this discrepancy is due to the prompt NO mechanism, which is not considered by *Miller* properly. There is a substantial gap between experimental data and numerical simulation for burning speed. This discrepancy may be due to the limited knowledge of fundamentals like thermal radiation, and fluid mechanical process within porous media.

Received : 30th September 2006 ; Accepted : 10th June 2007

REFERENCES

[1] Hsu, P. F. and Matthews, R. D., *Combustion and Flame*, **93**, 457 (1993).

[2] Zhou, X. Y. and Pereira, J. C., *Fire and Materials*, **22**, 187 (1998).

[3] Diamantis, D. J., Mastorakos, E. and Goussis, D. A., *Combustion Theory and Modeling,* **6**, 383 (2002).

[4] Howell, J., Hall, M. and Ellzey, J., *Progress Energy Combustion Science*, **22**, 121 (1996).

[5] Viskanta, R., "Handbook of Porous Media", 2nd Ed., Edited by K. Vafai, Taylor and Francis, Boca Raton (2004).

[6] Chaffin, C. Koening, M., Koeroghlian, M., Matthews, R., Hall, M., Nichols, S. and Lim, I., Proceeding of the ASME/JSME Thermal Engineering Joint Conference, Spring AFRC Meeting, Hartford, 4, 219 (1991).

[7] Leonardi, S. A., Viskanta, R. and Gore, J. P., *J. Heat Transfer*, **125**, 118 (2003).

[8] Modest, M. F., "Radiative Heat Transfer", McGraw-Hill Book Co., New York (1993).

[9] Kee, R.J., Mille, J. and Jefferson, T., Sandia National Laboratory Report SAND 80-8003 (1980).

[10] Miller, J. and Bowman, C. T., *Progress Energy Combustion Science*, **15**, 287 (1989).

[11] http://www.me.berkeley.edu/gri_mech/.

[12] Homma, R. and Chen, J. Y., ASPACC (1999).

[13] SUNG, C. J., LAW, C. K. and CHEN, J. Y., *Combustion and Flame*, **125**, 906 (2001).

[14] Cannon, S. M., Brewster, B. S. and Smoot, L. D., *Combustion and Flame*, **113**, 135 (1998).

[15] Glarborg, B., Lilleheie , N. I., Byggstoyl , S., Magnussen, B. F., Kilpinen, P. and Hupa, M., 24th Symposium In Combustion (International), The Combustion Institute, Pittsburg, PA, 889 (1992).

[16] Khosravy El-Hossaini, M., PhD Thesis, Faculty of Engineering, Tarbiat Modares University, Tehran, Iran (2007).